# Drag of Wings with Cambered Airfoils and Partial Leading-Edge Suction

James DeLaurier*
*University of Toronto, Downsview, Ontario, Canada*

**Traditional methods for wing drag calculation can greatly underestimate the maximum lift/drag ratios of low Reynolds number wings with highly cambered airfoils. The present work gives an alternative method that accounts for camber and leading-edge suction efficiency. Various results are drawn from this, including the conclusion that for zero leading-edge suction, an airfoil may be cambered so as to match the lift/drag ratio of a wing with 100% leading-edge suction, at a given lift coefficient. Also shown is an explanation of the parabolic drag behavior of two-dimensional airfoils in terms of partial leading-edge suction. Two comparisons with experiment are made which appear to confirm the reality of the analytical model and show the usefulness of this method for drag prediction.**

## Nomenclature

| | |
|---|---|
| $\mathcal{R}$ | = wing aspect ratio |
| $c$ | = airfoil chord |
| $C_c$ | = chordwise force coefficient, Eq. (5) |
| $C_d$ | = airfoil drag coefficient |
| $(C_d)_f$ | = airfoil skin-friction drag |
| $C_D$ | = finite-wing drag coefficient |
| $C_{D_f}$ | = skin-friction drag coefficient on finite wing |
| $C_{D_i}$ | = $C_D - C_{D_f}$ |
| $C_{D_p}$ | = finite-wing profile-drag coefficient |
| $C_L$ | = finite-wing lift coefficient |
| $C_{L_\alpha}$ | = $dC_L/d\alpha$ |
| $C_n$ | = wing or airfoil normal-force coefficient |
| $C_{n_\alpha}$ | = $dC_n/d\alpha$ |
| $C_{n_0}$ | = $C_{n_\alpha}\alpha_0$ |
| $(C_n)_d$ | = design value of $C_n$ |
| $C_s$ | = coefficient of chordwise leading-edge suction |
| $h$ | = maximum camber-line height from chord line |
| $x$ | = airfoil chordwise coordinate, aft from leading edge |
| $z$ | = airfoil normal coordinate, up from chord line |
| $U$ | = freestream velocity |
| $\alpha$ | = chord-line angle of attack to freestream velocity |
| $\alpha'$ | = chord-line angle of attack to downwash-deflected freestream velocity |
| $\alpha_i$ | = downwash-induced angle of attack, $\alpha - \alpha'$ |
| $\alpha_0$ | = angle between chord line and zero-lift line |
| $\gamma$ | = chordwise-distributed vorticity |
| $\gamma_1$ | = $\gamma$ for cambered airfoil at $\alpha' = 0$ |
| $\gamma_2$ | = $\gamma$ for flat-plate airfoil at angle $\alpha'$ |
| $\eta$ | = ratio of actual $C_s$ to theoretically maximum $C_s$ |

## Introduction

THIS work was motivated by the requirement to accurately estimate the drag of finite wings with highly-cambered airfoils operating at low Reynolds numbers ($\cong 10^5$). The traditional approach for wing drag estimations is described by Schlichting and Truckenbrodt[1] where, for a spanwise-elliptical lift distribution, the drag coefficient is given by

$$C_D = C_{D_p} + C_L^2/(\pi \mathcal{R}) \tag{1}$$

The second right-hand term, the "induced drag," is interpreted as the drag due to the lift of the finite wing; and the first term, the profile drag, is the two-dimensional drag of the wing's representative airfoil section. Perkins and Hage[2] state that $C_{D_p}$ has the form:

$$C_{D_p} = (C_{D_p})_{\min} + K'' C_L^2 \tag{2}$$

so that Eq. (1) may be rewritten as

$$C_D = (C_{D_p})_{\min} + C_L^2/(\pi \mathcal{R} e) \tag{3}$$

where $e$ is a constant efficiency factor.

Roskam[3] gives an interpretation of profile drag as being due to skin friction and partial leading-edge suction, so that $e$ may be expressed as

$$e = \frac{C_{L_\alpha}/\mathcal{R}}{\eta C_{L_\alpha}/\mathcal{R} + (1-\eta)\pi} \tag{4}$$

where $\eta$ is the leading-edge suction efficiency ($\eta = 1$ is 100% leading-edge suction). Note, however, that this assumes zero camber, which is also implied by Eq. (2) since the purpose of camber is to provide the minimum drag value at a finite lift.

With nearly 100% leading-edge suction and moderate camber, the preceding equations generally give adequate estimates for wing drag. However, note that $\eta$ can be much less than 1 at low Reynolds numbers according to Figure 3.14 of Ref. 3, which gives $\eta$ as a function of Reynolds number based on leading-edge radius. With high camber, then, these equations would significantly misrepresent the drag behavior and greatly underestimate the maximum values of $C_L/C_D$.

Such low Reynolds number airfoils were tested by Schmitz,[4] who showed that a sharp leading edge can improve normal-force performance by encouraging boundary-layer transition, and that a fairly high camber was required for good overall performance. The purpose of this study, then, is to provide an analytical insight into how camber benefits such airfoils with low leading-edge-suction efficiencies.

## Analysis and Results

### Analytical Model

A simple analytical model was chosen so that the results could be easily calculated and their significance not be obscured by excessive computational detail. It should therefore be noted that the results herein apply strictly to a model with the following assumptions: 1) incompressible flow; 2) un-

Received Aug. 30, 1982; revision received March 28, 1983.

*Associate Professor, Institute for Aerospace Studies. Member AIAA.

swept wing with elliptical spanwise loading; 3) airfoil sections with chordwise-symmetrical parabolic camber (for practical cambers, these are nearly circular arcs); and 4) small perturbations in the angle of attack and camber, so that thin-airfoil theory and lifting-line theory may be used for this analysis.

Despite these assumptions, it was felt that the results for this model would give quantitative insights into the function of camber for low-speed wings.

**Two-Dimensional Airfoil**

The chordwise circulation distribution on the airfoil shown in Fig. 1 is, to first order, the sum of the circulation on the cambered airfoil at $\alpha' = 0$, $\gamma_1$, plus that on a flat plate at angle $\alpha'$, $\gamma_2$, where from Schlichting and Truckenbrodt,[5]

$$\gamma_1 = 8U(h/c)\,[x(1-x)]^{1/2}$$

$$\gamma_2 = 2U\alpha'\,[(1-x)/x]^{1/2}$$

Note that these are for a unit chord.

The net chordwise force coefficient, without leading-edge suction, is given by

$$C_c = \frac{-2}{U}\int_0^1 \gamma(x)\,\frac{dz}{dx}\,dx \tag{5}$$

where the $\gamma_1$ distribution integrates to zero, and $\gamma_2$ into Eq. (5) gives

$$C_c = -2\pi(2h/c)\alpha' \tag{6}$$

Note also that the normal-force coefficient is given by

$$C_n = \frac{2}{U}\int_0^1 \gamma(x)\,dx \tag{7}$$

where $\gamma_1$ and $\gamma_2$ into Eq. (7) results in

$$C_n = 2\pi(2h/c + \alpha') \tag{8}$$

so that the camber gives a $C_n$ value when $\alpha' = 0$.

Now consider the leading-edge suction. The Blasius theorem states that, for nonseparated potential flow, the net force on the airfoil $L$ must be perpendicular to $U$, and the leading-edge suction $T_s$ must be such as to do this. In coefficient form, and referring to Fig. 2, one has

$$C_s = C_n\alpha' + C_c \tag{9}$$

where, from Eqs. (6) and (8), this becomes

$$C_s = 2\pi\alpha'(\alpha') \tag{10}$$

With reference to Eq. (8), this shows that the leading-edge suction is generated only by the "flat-plate" vorticity $\gamma_2$ (as may also be seen from the fact that $\gamma_1 = 0$ at the leading edge, whereas $\gamma_2 = \infty$).

Upon noting that the real-fluid $C_s$ may be less than ideal, as observed by Roskam[3] and Carlson et al,[6] a leading-edge efficiency factor $\eta$ is introduced into Eq. (10) so that

$$C_s = \eta 2\pi\alpha'(\alpha') \tag{11}$$

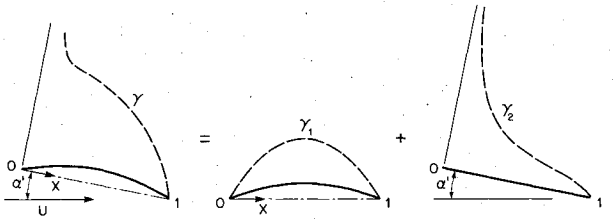


**Fig. 1 Airfoil circulation distributions.**

The airfoil's drag is assumed to be given by the skin-friction drag plus the net value of the streamwise components of the above forces; so that to first order one has

$$C_d = (C_d)_f + C_c - C_s + C_n\alpha' \tag{12}$$

which, from Eqs. (6), (8), and (11), further becomes

$$C_d = (C_d)_f + (1-\eta)2\pi(\alpha')^2 \tag{13}$$

This equation shows that for 100% leading-edge suction ($\eta = 1$), $C_d = (C_d)_f$ for all $\alpha'$ values; whereas for zero leading-edge suction ($\eta = 0$),

$$C_d = (C_d)_f + 2\pi(\alpha')^2 \tag{14}$$

This, in comparison with Eq. (8), shows that even for $\eta = 0$, the "camber lift" does not give a drag. This may be generalized by noting that $C_d = (C_d)_f$ for all $\eta$ values when $\alpha' = 0$ and $C_n = 4\pi h/c$. For the assumed airfoil, this corresponds to the "ideal" conditions described by Theodorsen,[7] where the flow smoothly enters the leading edge, giving a zero value of $\gamma$ at that point.

Therefore, one sees the value of camber in that, even for partial leading-edge suction, camber allows a finite lift to be generated (at $\alpha' = 0$) for which drag is due only to skin friction. Also, from Eq. (13), $C_d$ is a parabolic function of $C_n$ when $\eta < 1$. The fact that this behavior is seen in many two-dimensional airfoil data (such as in Ref. 4) may be attributed, in many cases, to their less than 100% leading-edge suction.

**Finite Wing**

For an unswept finite wing with elliptical spanwise loading, lifting-line theory, as described by Schlichting and Truckenbrodt,[1] gives a spanwise-constant induced angle of attack $\alpha_i$ where

$$\alpha_i = C_n/\pi AR \tag{15}$$

Therefore, as shown in Fig. 3, the wing's angle of attack to the relative wind is

$$\alpha' = \alpha - \alpha_i \tag{16}$$

and the wing's drag without skin friction is

$$C_{D_i} = C_c - C_s + C_n\alpha \tag{17}$$

where, with Eqs. (6), (8), (11), and (16), this becomes

$$C_{D_i} = (1-\eta)2\pi(\alpha')^2 + C_n\alpha_i \tag{18}$$

Note that $2h/c$ is the angle of the zero-lift line with respect to the chord $\alpha_0$ as shown in Fig. 3. Therefore Eq. (8) may be rewritten to give

$$2\pi\alpha' = C_n - 2\pi\alpha_0 \tag{19}$$

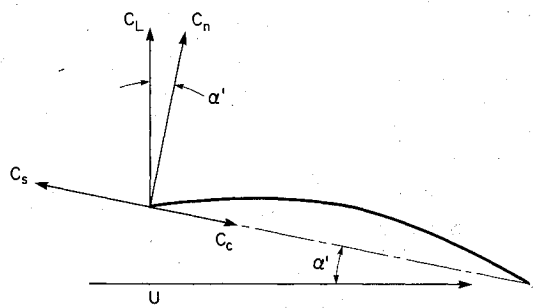


**Fig. 2 Force diagram on two-dimensional airfoil.**

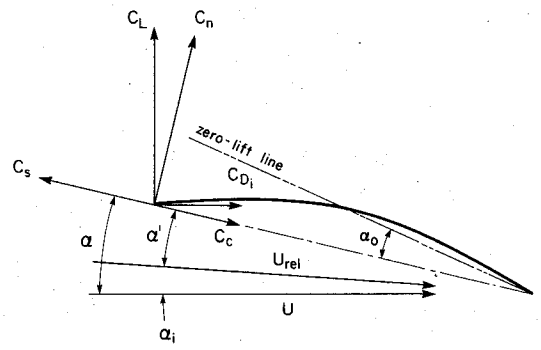


**Fig. 3 Angles and forces on finite-wing airfoil.**

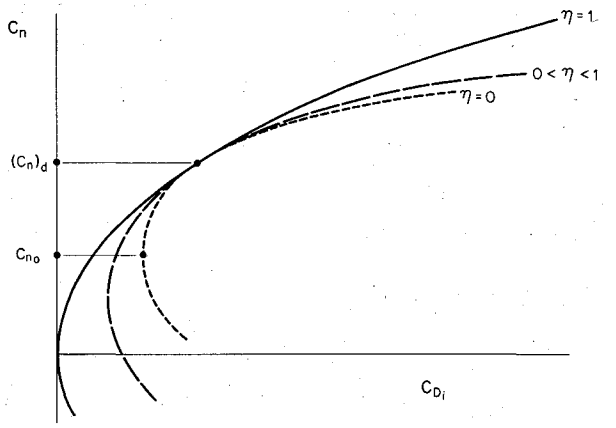


**Fig. 4 Finite-wing frictionless drag for various $\eta$ values.**

This, with Eqs. (15) and (16) substituted into Eq. (18), gives

$$C_{D_i} = \eta \frac{C_n^2}{\pi \mathcal{R}} + (1-\eta)\left(C_n\alpha - 2\pi\alpha_0\alpha + 2\alpha_0 \frac{C_n}{\mathcal{R}}\right) \tag{20}$$

Also, $C_n$ may be expressed as

$$C_n = C_{n_\alpha}(\alpha_0 + \alpha) \tag{21}$$

where, from Ref. 1

$$C_{n_\alpha} = 2\pi/(1 + 2/\mathcal{R}) \tag{22}$$

With these, Eq. (20) may be rewritten as

$$C_{D_i} = \eta \frac{C_n^2}{\pi \mathcal{R}} + (1-\eta)\left(\frac{C_n^2}{C_{n_\alpha}} - 2\alpha_0 C_n + 2\pi\alpha_0^2\right) \tag{23}$$

from which one may obtain the following results:

1) For 100% leading-edge suction ($\eta = 1$),

$$C_{D_i} = C_n^2/(\pi \mathcal{R}) \tag{24}$$

which is the classical induced-drag result, and is independent of camber.

2) For zero leading-edge suction ($\eta = 0$) and zero camber ($\alpha_0 = 0$),

$$C_{D_i} = C_n^2/C_{n_\alpha} \tag{25}$$

which is basically the result obtained from Eqs. (3) and (4) when $\eta = 0$.

3) For zero leading-edge suction ($\eta = 0$) and finite camber ($\alpha_0 \neq 0$),

$$C_{D_i} = C_n^2/C_{n_\alpha} - 2\alpha_0 C_n + 2\pi\alpha_0^2 \tag{26}$$

from which the $C_n$ for minimum $C_{D_i}$ is

$$\text{Minimum drag } C_n = C_{n_\alpha}\alpha_0 \equiv C_{n_0} \tag{27}$$

and the corresponding $C_{D_i}$ value is

$$(C_{D_i})_{\min} = (2\pi/C_{n_\alpha} - 1)C_{n_0}^2/C_{n_\alpha} \tag{28}$$

Note how this varies quadratically with $C_{n_0}$ so that a finite drag exists at $\alpha = 0$ for all nonzero cambers. The above results clearly show the advantage of camber when $\eta = 0$. However, it should still be noted that $C_{D_i}$ at $C_{n_0}$ is even less when $\eta = 1$, as may be seen when Eq. (22) is used to rewrite Eq. (24) as

$$(C_{D_i})^{\eta=1} = (2\pi/C_{n_\alpha} - 1)C_n^2/2\pi \tag{29}$$

From Eq. (22), $C_{n_\alpha} < 2\pi$, so that upon comparing Eqs. (28) and (29) when $C_n = C_{n_0}$, one sees that

$$(C_{D_i})^{\eta=1} < (C_{D_i})^{\eta=0}_{min} \tag{30}$$

These results are illustrated in Fig. 4.

4) For partial leading-edge suction ($\eta < 1$) and finite camber ($\alpha_0 \neq 0$), $C_{D_i}$ is given by Eq. (23). If a wing of given $\mathcal{R}$ is required to fly at a given "design value" of normal-force coefficient, $(C_n)_d$, Eq. (23) may be used to find the camber (represented by $\alpha_0$) required to minimize $C_{D_i}$:

$$dC_{D_i}/d\alpha_0 = 0 \quad \text{which gives} \quad \alpha_0 = (C_n)_d/2\pi \tag{31}$$

and the corresponding value of $C_{D_i}$ is

$$(C_{D_i})_d = (C_n)_d^2/\pi \mathcal{R} \tag{32}$$

Note that this is independent of $\eta$ and equal to the $C_{D_i}$ for the $\eta = 1$ case [Eq. (24)], for that given $(C_n)_d$. Therefore, a wing with partial leading-edge suction can be designed to give as low a $C_{D_i}$ as that for a wing with 100% leading-edge suction, for a given value of $C_n$, if the camber is adjusted according to Eq. (31). Again, note that this corresponds to the "ideal" conditions defined by Theodorsen,[7] where each airfoil along the span is operating with zero circulation at its leading edge.

Next, one may find the drag difference between the $\eta = 1$ and $\eta < 1$ cases for $C_n \neq (C_n)_d$ by defining

$$\Delta C_D = (C_{D_i})_{\eta<1} - (C_{D_i})_{\eta=1}$$

which, from Eq. (23), becomes

$$\Delta C_D = (\eta - 1)\frac{C_n^2}{\pi \mathcal{R}} + (1-\eta)\left(\frac{C_n^2}{C_{n_\alpha}} - 2\alpha_0 C_n + 2\pi\alpha_0^2\right) \tag{33}$$

As before, $\Delta C_D = 0$ when $C_n = (C_n)_d$. Further, note that $d(\Delta C_D)/dC_n$ also equals zero when $C_n = (C_n)_d$, which shows that the slopes of the $C_{D_i}$ vs $C_n$ polar curves for the $\eta = 1$ and $\eta < 1$ wings are equal where they touch at $(C_n)_d$. Finally, the second derivative,

$$\left[\frac{d^2(\Delta C_D)}{dC_n^2}\right]_{C_n=(C_n)_d} = \frac{(1-\eta)}{\pi} \tag{34}$$

is positive, which, along with the previous results, shows that $\Delta C_D$ is always positive when $C_n \neq (C_n)_d$. Therefore, the "off design" drag of the $\eta < 1$ wing is always greater than that for the $\eta = 1$ wing. These results are represented in Fig. 4. Finally, note that, with Eq. (22), Eq. (23) may be rewritten as

$$C_{D_i} = \frac{C_n^2}{\pi \mathcal{R}} + (1-\eta)\left(\frac{C_n^2}{2\pi} - 2\alpha_0 C_n + 2\pi\alpha_0^2\right) \tag{35}$$

where the second right-hand term is the two-dimensional airfoil's frictionless drag, $C_d - (C_d)_f$. Therefore, the wing's total drag may be expressed as

$$C_D = \frac{C_n^2}{\pi \mathcal{R}} + C_d \tag{36}$$

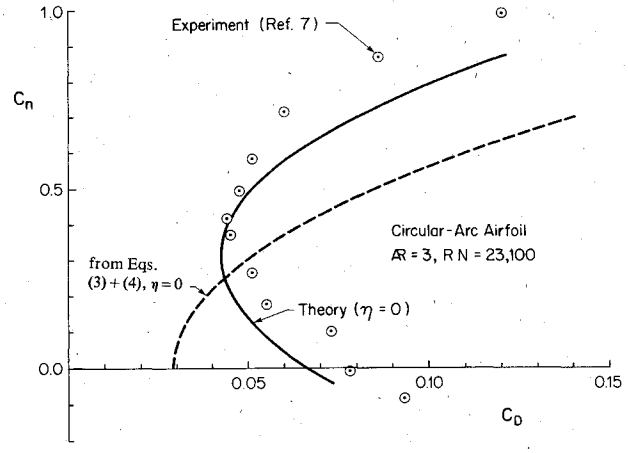


**Fig. 5 Drag polar for a wing with a circular-arc airfoil.**

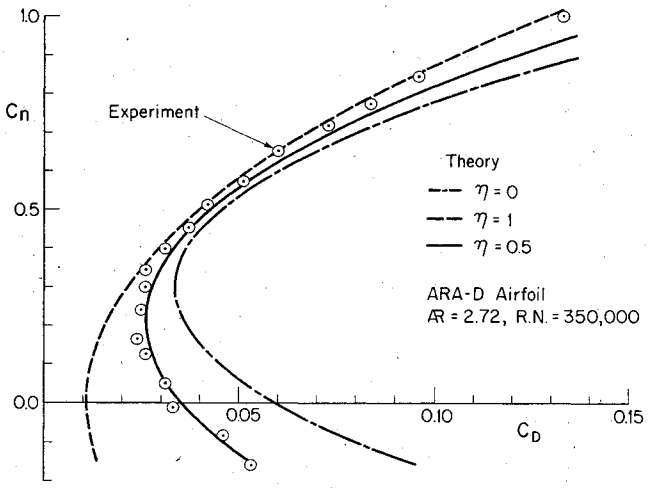


**Fig. 6 Drag polar for a wing with an ARA-D airfoil.**

which is the same as Eq. (1), with $C_{D_p} = C_d$ and $C_L \approx C_n$. This shows that, even with camber and partial leading-edge suction, one may use the traditional approach for wing drag estimation, provided that the profile drag is accurately expressed.

## Comparisons of Theory with Experiment

An evaluation of this analysis was provided by calculating the drag polars of two thin highly-cambered wings for which experimental results exist. One of these, obtained from DeLaurier and Harris,[8] has a rectangular planform of $\mathcal{R} = 3$ and a thin circular-arc airfoil of 6.7% camber. The chordwise Reynolds number was 23,100 and the leading edge was sharp, so that from Fig. 3.14 of Ref. 3, zero leading-edge suction ($\eta = 0$) was assumed.

A least-squares linear fit of the $C_n$ vs $\alpha$ data for $-5$ deg $\lesssim \alpha \lesssim 9$ deg gave $C_{n_\alpha} = 4.0279$/rad and $\alpha_0 = 0.0774$ rad. These, into Eq. (23), gave $C_{D_i}$, to which was added the friction drag, assumed to be the zero-angle drag of a zero-camber airfoil from the same series of experiments: $C_{D_f} = 0.029$. Thus the total drag coefficient is given by

$$C_D = 0.0666 - 0.1548C_n + 0.2483C_n^2 \tag{37}$$

This function is plotted with experimental results in Fig. 5. The comparison is favorable in that both have their minimum drag at nonzero lift coefficients; beyond this point, the general trends are very similar. The relative vertical displacement between the two polars (of $\Delta C_n \cong 0.1$) may be due to unavoidable errors in setting the wing's angle of attack (it only had a 2 in. chord; also, lift and drag were measured separately in two different runs). Note, however, the considerable error when $C_D$ is calculated from Eqs. (3) and (4), as shown in Fig. 5. The present analysis agrees much more closely with the experimental results.

A second example is provided by experiments performed by Wong and Uffen on a rectangular-planform wing of $\mathcal{R} = 2.72$ with a modified ARA-D airfoil, whose ordinates, supplied by W.R. Morgan of Aero Vironment Inc., give a 5.75% maximum camber located 50% aft from the leading edge and a maximum thickness of 6.41% located 21% aft from the leading edge. The chordwise Reynolds number was 350,000 and the nominal leading-edge radius is $\cong 1.3\%$. Therefore, the leading-edge Reynolds number $\cong 4500$ which, from Fig. 3.14 of Ref. 3, gives an $\eta \cong 0.5$.

A least-squares linear curve fit of the $C_n$ vs $\alpha$ data for $-6$ deg $\lesssim \alpha \lesssim 6$ deg gave $C_{n_\alpha} = 3.400$/rad and $\alpha_0 = 0.0655$ rad. Also, zero-angle tests at the same Reynolds number on a thin uncambered wing constructed in the same fashion gave a frictional drag coefficient of $C_{D_f} = 0.0110$, so that this plus Eq. (23) give the following total-drag expressions:

$$\text{For } \eta = 0, \quad C_D = 0.0110 + 0.1172C_n^2 \tag{38}$$

$$\text{For } \eta = 1, \quad C_D = 0.0602 - 0.1770C_n + 0.2941C_n^2 \tag{39}$$

$$\text{For } \eta = 0.5, \quad C_D = 0.0356 - 0.0885C_n + 0.2057C_n^2 \tag{40}$$

These are plotted with the data in Fig. 6, from which it is seen that the $\eta = 0.5$ curve matches closely within the $0 \lesssim C_n \lesssim 0.6$ range, which corresponds to $-5.07$ deg $\lesssim \alpha \lesssim 5.04$ deg. From this one may conclude, first, that the $\eta = 0.5$ value is a reasonable estimate, although a slightly larger value would give a better match. Second, it appears that this theory may be usefully applied to airfoils which differ, to first order, from thin circular arcs. Note that the above-mentioned $\alpha$ range is consistent with the linearized assumptions of this theory, and that this range includes the $\alpha$ for maximum $C_n/C_D$ (2.01 deg for $C_n/C_D = 12.3$).

Finally, the three curves do not touch at a common $(C_n)_d$ because $C_{n_\alpha}$ was obtained from the experimental data instead of Eq. (22), which is not accurate at low aspect ratios. However, the reasonable match between theory and experiment indicates that although Eq. (22) was used in the derivation of Eq. (23), one should use the most accurate $C_{n_\alpha}$ value in Eq. (23), however obtained.

## Discussion

A major assumption in this analysis is that any flow separation is confined to the leading edge, where it may act to reduce the chordwise leading-edge suction from its full theoretical value. Elsewhere along the chord the flow is assumed to be totally attached. For the low Reynolds numbers implied in this work, this limits the angle-of-attack range to fairly low magnitudes, such as $-5$ deg $\lesssim \alpha \lesssim 10$ deg. Also, note that $\eta$ and $(C_d)_f$ are assumed to be constant throughout this range.

The assumption that the airfoil has chordwise-symmetrical parabolic camber would appear to limit this analysis to airfoils which, for practical camber magnitudes, have essentially circular-arc camber lines. However, note that camber is represented in Eq. (23) by $\alpha_0$, which suggests that Eq. (23) may be usefully applied to airfoils with more traditional camber lines and known values of $\alpha_0$. The experiments on the wing with the ARA-D airfoil appear to confirm this notion.

Subject to the assumptions, the essential results from this work are that, first, with 100% leading-edge suction, camber has no effect on the frictionless drag, so that an airfoil's "profile drag" is due only to friction, and a wing's "induced drag" is given by the classical Eq. (1). Next, with partial leading-edge suction, a two-dimensional airfoil's "profile

drag" has a parabolic component, aside from any skin-friction contributions, given by Eq. (13). Also a finite-wing's frictionless drag, calculated from Eq. (23), is larger than that for an identical wing with 100% leading-edge suction, with the exception of a single "design point" where the normal-force coefficient and camber are related by Eq. (31). At this point, the cambered wing's performance is independent of leading-edge suction, which shows the essential advantage of camber when a desired operating value of normal-force coefficient can be specified.

An obvious conclusion from these results would appear to be that the leading edge should be shaped so as to attain as high a leading-edge suction efficiency as possible. This would minimize the drag increment [defined in Eq. (33)] for flight conditions away from the design point. However, as discussed in the introduction, certain low-Reynolds-number airfoils benefit from sharp leading edges and camber. This work gives an analytical insight into why this is so, as well as indicating the amount of camber required.

## Concluding Remarks

The analysis described in this paper gives a method by which one may estimate the frictionless drag of wings with cambered airfoils and partial leading-edge suction. Subject to the geometric and aerodynamic assumptions made, the results show how camber greatly benefits a wing's performance when its leading-edge suction is less than 100%. Although the frictionless drag of such a wing will never be less than that for 100% leading-edge suction, a specific "design point" may be identified at which the drags are equal for a given normal-force coefficient.

Comparisons with experimental results on two low-Reynolds number wings appear to confirm the theoretical method's usefulness for drag prediction. This was particularly encouraging in that one of these wings had both airfoil geometry and aspect ratio which differed significantly from those assumed in the theory's physical model.

Future work could generalize the assumed wing geometries; but the most useful direction may be to study, in detail, leading-edge suction and the mechanism of its being only partially attained.

## Acknowledgments

This work was supported through a research contract from the Canadian Department of Communications, Communications Research Centre, and an Operating Grant from the Natural Sciences and Engineering Research Council of Canada. The wind tunnel experiments on the wing with the ARA-D airfoil were performed by John Wong, a Research Associate at UTIAS, and Donald Uffen, a Research Assistant at UTIAS. Also, this analysis benefited greatly from the careful study and helpful suggestions of J.M. Harris, Principal Research Engineer at Battelle Memorial Institute.

## References

[1] Schlichting, H. and Truckenbrodt, E., "Wings of Finite Span in Incompressible Flow," *Aerodynamics of the Airplane,* Translated by Heinrich Ramm, McGraw-Hill Book Co., New York, 1979, pp. 112-123.

[2] Perkins, C.D. and Hage, R.E., "Drag Estimation," *Airplane Performance Stability and Control,* 8th printing, John Wiley & Sons, New York, 1960, pp. 90-96.

[3] Roskam, J., "Calculation of $(C_{D_i})_{WB}$," *Methods for Estimating Drag Polars of Subsonic Airplanes,* Univ. of Kansas, Lawrence, Kansas, 1971, pp. 3.18-3.19.

[4] Schmitz, F.W., "Aerodynamics of the Model Airplane. Part I —Airfoil Measurements," NASA TM-X-60976, Nov. 1967.

[5] Schlichting, H. and Truckenbrodt, E., "Airfoil of Infinite Span in Incompressible Flow (Profile Theory)," *Aerodynamics of the Airplane,* Translated by Heinrich Ramm, McGraw-Hill Book Co., New York, 1979, pp. 57-58.

[6] Carlson, H.W., Mack, R.J., and Barger, R.L., "Estimation of Attainable Leading-Edge Thrust for Wings at Subsonic and Supersonic Speeds," NASA Technical Paper 1500, Oct. 1979.

[7] Theodorsen, T., "On the Theory of Wing Sections with Particular Reference to the Lift Distribution," NACA Rept. 383, 1931.

[8] DeLaurier, J.D. and Harris, J.M., "Experimental Investigation of the Aerodynamic Characteristics of Stepped-Wedge Airfoils at Low Speeds," AIAA Paper 74-1015, Sept. 1974.